All-angle Negative Refraction and Active Flat Lensing in the Ultraviolet

Ting Xu[1,2], Amit Agrawal[1,3], Maxim Abashin[1,2], Kenneth J. Chau[4] and Henri J. Lezec[1]

[1]Center for Nanoscale Science and Technology, National Institute of Standard and Technology, Gaithersburg, MD 20899, USA

[2]Maryland Nano-Center, University of Maryland, College Park, MD 20742, USA

[3]Department of Electrical Engineering and Computer Science, Syracuse University, Syracuse, NY 13244, USA

[4]School of Engineering, The University of British Columbia V1V 1V7, Kelowna, British Columbia, Canada

Decades ago, Veselago[1] predicted that a material with simultaneously negative electric and magnetic polarization responses would yield a 'left-handed' medium in which light propagates with opposite phase and energy velocities—a condition described by a negative refractive index. He proposed that a flat slab of left-handed material possessing an isotropic refractive index of −1 could act like an imaging lens in free space. Left-handed materials are not naturally occurring, and it has only recently become possible to achieve a left-handed response using metamaterials, that is, electromagnetic structures engineered on subwavelength scales to elicit tailored polarization responses. So far, left-handed responses have typically been implemented using resonant metamaterials composed of periodic arrays of unit cells containing inductive–capacitive resonators and conductive wires. Negative refractive indices that are isotropic in two[2] or three[3] dimensions at microwave frequencies have been achieved in resonant metamaterials with centimetre-scale features. Scaling the left-handed response to higher frequencies, such as infrared or visible, has been done by shrinking critical dimensions to submicrometre scales by means of top-down nanofabrication[4]. This miniaturization has, however, so far been achieved at the cost of reduced unit-cell symmetry, yielding a refractive index that is negative along only one axis. Moreover, lithographic scaling limits have so far precluded the fabrication of resonant metamaterials with left-handed responses at frequencies beyond the visible[5]. Here we report the experimental implementation of a bulk metamaterial with a left-handed response in the ultraviolet. The structure, based on stacked plasmonic waveguides[6], yields an omnidirectional left-handed response for transverse magnetic polarization characterized by a negative refractive index. By engineering the structure to have a refractive index close to −1 over a broad angular range, we achieve Veselago flat lensing, in

free space, of arbitrarily shaped, two-dimensional objects beyond the near field. We further demonstrate active, all-optical modulation of the image transferred by the flat lens.

The electric and magnetic polarization responses of a linear, isotropic medium are described using two scalar constitutive parameters - the complex permittivity, $\underline{\varepsilon} = \varepsilon' + i\varepsilon''$, and the complex permeability, $\underline{\mu} = \mu' + i\mu''$. The physics of time-harmonic electromagnetic wave propagation in such a medium can be derived from Maxwell's equations and distilled into the form of plane-wave solutions. Plane waves are characterized by a wavevector, *k*, and a time-averaged Poynting vector, *S*, which respectively give the directions of phase velocity and energy flow in the medium. In an isotropic medium, *k* and *S* are always collinear, but are either parallel or antiparallel, following the causality condition[7] $\mathrm{sgn}(k \bullet S) = \mathrm{sgn}(\alpha)$, where $\alpha = \varepsilon' |\underline{\mu}| + \mu' |\underline{\varepsilon}|$. A general index of refraction given by $n = \mathrm{sgn}(\alpha) |\mathrm{Re}(\sqrt{\underline{\mu}\underline{\varepsilon}})|$ can then be introduced, which describes both the magnitude of *k* with respect to its value in free space ($|k| = |n| k_0 = |n| \omega / c$, where ω is the frequency and *c* is the speed of light) as well as the relative direction of *k* and *S*. For a material in which $\alpha > 0$—called 'right-handed' because *k* and *S* are parallel ($k \bullet S > 0$)—the index of refraction is positive. Plane waves in right-handed media propagate with wavefronts streaming along the direction of energy flow, similar to a wave in free space. The archetypal right-handed medium is a 'double-positive' material such as air or glass, for which ε' and μ' are simultaneously positive. In the contrasting case of a material in which $\alpha < 0$—called 'left-handed' because *k* and *S* are antiparallel ($k \bullet S < 0$)—the index of refraction is negative. Plane waves in left-handed media propagate as an exotic 'backwards wave' with wavefronts travelling in a direction opposite to that of energy flow. The classical left-handed medium, first introduced by Veselago, is the 'double-negative' one, for which ε' and μ' are simultaneously negative.

Plane-wave refraction at the boundary of a left-handed medium can be modelled using Snell's law, under the convention that its refractive index takes negative values. Conservation of phase and energy flow applied to a plane wave crossing the boundary between a medium with index n_1 and another with index n_2 yields $n_1 \sin(\theta_1) = n_2 \sin(\theta_2)$, a generalized form of Snell's law in which n_1 and n_2 have arbitrary signs and θ_1 and θ_2 are the directed angles of the optical ray path with respect to the normal on each side of the interface. If n_1 and n_2 have opposite signs, then θ_1 and θ_2 have opposite signs and the ray deflects across the boundary to the same side of the normal—a phenomenon known as negative refraction. If n_1 and n_2 are equal in magnitude but opposite in sign, the ray path is perfectly mirrored about the interface. In the configuration of a flat slab, this type of negative refraction occurs at both interfaces and it becomes possible to focus a collection of rays from a point source to another point on the other side of the slab. As suggested by Veselago[1], a lens in free space could be realized by simply using a flat slab of material with an isotropic refractive index of -1.

The current limitations of top-down nanofabrication hinder straightforward implementation of metamaterials that are able to display a three-dimensionally isotropic, negative-index response at optical frequencies, using the canonical system of volumetric arrays of discrete, shape-based resonators with critical features and spacing of deep subwavelength dimensions[5] (that is, dimensions much smaller than half the wavelength). Metamaterials based on plasmonic waveguides consisting of alternating planar metal (M) and dielectric (D) layers offer an attractive alternative to achieving a high-frequency left-handed response[8–10]. This left-handed response is derived from a transverse-magnetic-polarized (TMP) backwards electromagnetic mode naturally sustained by the waveguide in a frequency range between the

bulk plasmon resonance frequency, ω_P, of the metal—typically located in the ultraviolet—and the surface plasmon resonance frequency, ω_{SP}, of the metal–dielectric interface, which can be positioned within the visible by proper choice of constituent materials. Using this approach, a metal–dielectric–metal (MDM) plasmonic waveguide with an ultrathin dielectric core was employed to achieve a two-dimensionally isotropic, negative refractive index at green and blue frequencies, as evidenced by observation of in-plane negative refraction[11]. Recently it was theoretically shown that a plasmonic-waveguide-based system could be devised in which the left-handed response is extended to an extra dimension normal to the plane of the layers[6]. The proposed metamaterial, which is composed of a stack of strongly coupled plasmonic waveguides each having an MDMDM layer sequence, was designed to have an in-plane mode symmetry that allows propagation of a TMP backwards wave in three dimensions at a visible wavelength of 400 nm.

Here we design a plasmonic waveguide metamaterial based on repeated MDMDM layered unit cells (Fig. 1a) to have an all-angle left-handed response in the ultraviolet characterized by a refractive index close to −1. With Ag (metal) and TiO_2 (dielectric) as the constituent materials, we use the transfer matrix method[12] to produce a three-dimensional equifrequency contour (EFC) at the ultraviolet wavelength $\lambda_0 = 363.8$ nm for transverse magnetic polarization (magnetic field parallel to the plane of the layers). The EFC maps the angular dependence of the wavevector in the metamaterial and indicates the direction of the Poynting vector (which is normal to the EFC and points in the direction of its displacement as a function of frequency). The individual layer thicknesses of the MDMDM layers comprising each unit cell (33, 28, 30, 28 and 33 nm, respectively) are optimized to achieve a broad-angle refractive index of −1, as evidenced by an EFC that has a near-spherical shape with a radius of

approximately k_0 (Fig. 1b) and moves inward with increasing frequency[13] (such that $k \bullet S < 0$). For a plane wave incident from free space onto the metamaterial at an incident angle θ_i, continuity of phase and conservation of energy at the interface dictate that the transmitted backwards wave has a wavevector k_t (pointing towards the interface) and a Poynting vector S_t (pointing away from the interface) on the same side of the normal as the incident ray path, conditions describing negative refraction of phase and power. Because the metamaterial EFC is not perfectly spherical, k_t and S_t are not exactly collinear and Snell's law, which applies to phase refraction, cannot be rigorously applied to refraction of power. To describe power refraction from free space into the metamaterial in a manner analogous to Snell's law, we introduce a power refractive index $n_S \equiv \sin(\theta_i)/\sin(\theta_{t,S})$, where $\theta_{t,S}$ is the directed angle between the path of power flow with respect to the normal.

A slab of the designed metamaterial is fabricated by sputtering three MDMDM unit cells (metal, Ag; dielectric, TiO_2) onto a transparent glass substrate, to a total thickness of approximately 450 nm, followed by patterning of an illumination aperture consisting of a 600-nm-wide rectangular opening in an opaque Cr film (Fig. 2a). To measure power refraction from free space into the metamaterial, we illuminate the aperture-masked, air-facing surface of the metamaterial at various incidence angles (θ_i) with continuous-wave radiation at $\lambda_0 = 363.8$ nm, and extract the angular deflection of beam power ($\theta_{t,S}$) from the lateral shift, *L*, of the most intense part of the exiting beam relative to the aperture centre. For transverse magnetic polarization, we observe negative power refraction of the ultraviolet beam over a broad range of incident angles spanning $10° \le \theta_i \le 60°$ (Fig. 2b). Power refraction switches from negative to positive when the polarization of the ultraviolet beam is rotated to a transverse electric

configuration (electric field parallel to the plane of the layers), a result expected owing to the absence of TMP plasmon modes to confer left-handed electromagnetic behaviour.

The power refractive index measured for transverse magnetic polarization is approximately −1 over a broad range of angles and closely matches expected values based on the curvature of the EFC of the designed metamaterial (Fig. 2c). There is also good agreement between measured power refraction and two virtual experiments performed with a finite-difference time-domain (FDTD) simulator solving Maxwell's equation: one which calculates the angular deflection of a beam through an aperture-bearing metamaterial akin to that in the experiments, and another which calculates the unit-cell-averaged Poynting vector in a bare metamaterial subject to plane-wave illumination (Fig. 2c). We extract the effective constitutive parameters of the bare metamaterial by applying a parameter retrieval technique to FDTD-simulated reflection and transmission data[14]. The effective refractive index, n_{eff}, is approximately −1 over a large angular range and agrees with the refractive index expected from the metamaterial EFC (Fig. 2d), confirming the realization of the designed omnidirectional left-handed response. The metamaterial has a double-negative response characterized by simultaneously negative values of ε' and μ' (Supplementary Fig. 1). In contrast with other metamaterial implementations that achieve visible-frequency left-handed behaviour from a single negative response[15] (in which one of ε' and μ' is negative), the double-negative response here enables low-loss wave propagation (evidenced by a relatively high figure of merit; Supplementary Fig. 1) beneficial for applications such as imaging.

Veselago flat lensing is a special refractory phenomenon that occurs when a flat slab of thickness d has an isotropic refractive index of −1 and is immersed in free space. In Fig. 3a, we depict the simplest form of Veselago flat lensing, in which diverging rays from a point object

positioned on one of the faces of the slab are refracted at the opposite face and focused to a point image a distance *d* beyond the slab. Experimental demonstrations of Veselago flat lensing have so far only been possible at microwave frequencies, for which bulk left-handed metamaterials with two- or three-dimensionally isotropic, negative refractive indices are available[3,16–18]. Here we exploit the broad-angle negative refractive index achieved with our left-handed metamaterial to demonstrate Veselago flat lensing in the ultraviolet, extending the experimental realization of this effect across the electromagnetic spectrum and into a frequency range with important applications such as fluorescence imaging and photolithography. Although our metamaterial has a left-handed response only for transverse magnetic polarization, we show that imaging with circular polarization enables a flat slab of the metamaterial to perform three-dimensional imaging of two-dimensional objects beyond the near field ($d > \lambda_0$), closely approximating ideal, far-field flat lensing discussed by Veselago..

The flat lens consists of a free-standing film of the stacked-waveguide metamaterial described and characterized above. To probe the performance of the lens, imaging apertures of various shapes are fabricated directly on the lens surface. The apertures are illuminated at normal incidence with coherent ultraviolet light ($\lambda_0 = 363.8$ nm), replicating the schematic set-up in Fig. 3a. The lensing performance of the structure is first characterized by using it to image a slit aperture of width w_s = 180 nm, illuminated by TMP light (magnetic field oriented along the slit). The lateral intensity profile of the transmitted light on the opposite side of the metamaterial slab is recorded with an optical microscope as a function of distance, *z*, relative to the exit surface of the slab (Fig. 3b), where $z > 0$ corresponds to a position outside the slab. A curve fit to the full-width at half-maximum (FWHM) of the intensity profile reveals a beam waist located at a position $z_f = 390$ nm, which is interpreted as the focal distance of the flat lens relative to the lens

exit surface. The measured focal distance is comparable to the theoretical value of 450 nm expected for a flat lens consisting of an ideally isotropic left-handed medium of refractive index $n = -1$ and thickness $d = 450$ nm. In addition, z_f is consistent with the numerical value of 360 nm predicted by an FDTD simulation of the stacked-waveguide metamaterial lens bearing a slit aperture (Fig. 3b, inset). The experimentally measured beam width at z_f has a FWHM value of $w_{f,Meas} \approx 370$ nm, which is limited by the resolution of the optical microscope used for the observation. The FDTD simulations yield a minimum beam width of $w_{f,FDTD} = 200$ nm, which is close to the theoretical resolution limit of the implemented flat lens (Supplementary Fig. 2).

Although image transfer with no loss of spatial frequencies beyond the diffraction limit (super-resolution) was derived for the ideal case of a lossless, non-dispersive Veselago flat lens with $\varepsilon = \mu \equiv -1$ (ref. 19), imaging performance under more realistic conditions of loss, dispersion or even infinitesimal departure from rigorous equality between ε and μ has been shown to be significantly degraded[20,21]. In particular, near-complete loss of super-resolution is expected when a lossy, dispersive left-handed Veselago flat lens of super-wavelength thickness ($d \geq \lambda_0$, as here) is used for image transfer beyond the near field[16,22–24]. Though image transfer with a finite amount of super-resolution has been experimentally demonstrated in recent years at ultraviolet frequencies comparable to that of the present experiment using a non-left-handed 'poor-man's' superlens consisting of a thin, flat Ag film[25] ($d \approx \lambda_0 / 12$), this electrostatic-limit imaging mode is possible only over near-field distances, a situation which is conceptually different from that of the present study.

The ability of the fabricated flat lens to image two-dimensional objects of arbitrary shapes is demonstrated using cross (Fig. 3c) and ring (Fig. 3d) slit apertures. The aperture width

is set to a constant value of 180 nm ($w_s < \lambda_0 / 2$) to suppress transverse-electric-polarized light, which is not focused by the lens. To maintain imaging of the full specified shapes of the two-dimensional aperture objects, circularly polarized illumination is used to probe evenly all radial directions of each object. The resulting images of the objects formed by the flat lens are shown in Fig. 3e (cross) and Fig. 3f (ring), as recorded by the optical microscope focused at z_f. The salient characteristics of the images, including point-to-point replication of features of the two-dimensional objects, are consistent with those expected from a Veselago flat lens imaging beyond the near field.

In parallel with their exotic refractive properties, actively tunable metamaterials offer the possibility of dynamic control of light[26]. Here we demonstrate that the intensity of an ultraviolet image transferred by the metamaterial flat lens (for continuous-wave illumination at $\lambda_0 = 363.8$ nm) can be dynamically varied by illumination of the exit surface of the lens with a pulsed pump beam ($\lambda_{pump} = 290$ nm) tuned above the bandgap of the as-deposited constituent TiO_2 (characterized in Supplementary Fig. 3). As the pump intensity, I_{pump}, is increased, the transmitted intensity, I_{ON}, is observed to decrease (Fig. 3g). The corresponding intensity modulation contrast, $\gamma = (I_{OFF} - I_{ON}) / I_{OFF}$ (where I_{OFF} is the transmitted intensity in the absence of pumping), displays a quasilinear dependence on I_{pump} and increases to a value of $\gamma \approx 50\%$ at the maximum explored pump intensity below the damage threshold of the sample. Conversely, pumping the metamaterial to similar intensities at a wavelength tuned below the TiO_2 bandgap ($\lambda_{pump} = 760$ nm) yields no significant transmission modulation ($\gamma \approx 0\%$). These observations support the hypothesis that pump-induced transmission suppression results from absorption by

free carriers generated in the TiO_2 (refs 27, 28). The achieved modulation contrast exceeds that of electro-absorption-based solid-state devices operating in the ultraviolet[29,30].

We have experimentally demonstrated a bulk metamaterial with an all-angle negative index of refraction, and have used it to achieve Veselago flat lensing and all-optical modulation in the ultraviolet. The fabrication-friendly planar architecture of this metamaterial shows promise for building large-area left-handed optical elements for manipulating light at frequencies beyond the visible.

METHODS SUMMARY

To fabricate the structure used for the refraction experiment, sequential direct-current and radio-frequency sputtering in the same sputter chamber were used to deposit alternating layers of Ag and TiO_2 on a transparent glass slide (deposition rates: $R_{Ag} \approx 3.6$ Å s^{-1}, $R_{TiO_2} \approx 0.35$ Å s^{-1}). The resulting metamaterial was then sputter-coated with a 120-nm-thick Cr layer, with an aperture etched through the Cr layer using FIB milling. Finally, two reference alignment marks consisting of 100-nm-wide, 1-μm-long slits through the full thickness of the metamaterial down to the glass substrate were also patterned by FIB milling in the vicinity of the aperture. The structure used for the flat-lensing experiment was fabricated by sputter deposition of a metamaterial stack onto a Si_3N_4 membrane previously coated with a 120-nm-thick Cr layer. FIB milling was then used from the membrane side to remove the Si_3N_4 locally and pattern various slit-aperture objects through the Cr layer.

For both refraction and lensing experiments, accurate referencing of the focal plane of the optical microscope (with a ×100 objective lens) relative to the exit surface of the metamaterial was achieved by focusing the diverging ultraviolet light emitted by the alignment-mark slits on the exit surface. In addition, the illuminated alignment marks were also used as a reference for accurate calibration of the lateral shift of the transmitted beam under refraction at various angles of incidence. For the active flat-lensing experiment, a ×40, deep-ultraviolet objective lens was used to record the probe beam and simultaneously focus the pump beam onto the sample surface. After each pump-on experiment, the transmitted intensity of the probe beam was rechecked to exclude the possibility of the flat lens sample being damaged during the pump process.

References

1. Veselago, V. G. The electrodynamics of substances with simultaneously negative values of of ε and μ. *Sov. Phys. Usp.* **10**, 509-514 (1968).
2. Shelby, R. A., Smith, D. R. & Schultz, S. Experimental verification of a negative index of refraction. *Science* **292**, 77-79 (2001).
3. Rudolph, S. M. & Grbic, A. A broadband three-dimensionally isotropic negative-refractive-index medium. *IEEE Trans. Antennas. Propag.* **60**, 3661-3669 (2012).
4. Shalaev, V. M. Optical negative-index metamaterials. *Nature Photon.* **1**, 41-48 (2007).
5. Soukoulis, C. M. & Wegener, M. Past achievements and future challenges in the development of three dimensional photonic metamaterials. *Nature Photon.* **5**, 523-530 (2011).
6. Verhagen, E., Waele, R. D., Kuipers, L. & Polman, A. Three-dimensional negative index of refraction at optical frequencies by coupling plasmonic waveguides. *Phys. Rev. Lett.* **105**, 223901 (2010).
7. Depine, R. A. & Lakhtakia, A. A new condition to identify isotropic dielectric-magnetic materials displaying negative phase velocity. *Microw. Opt. Technol. Lett.* **41**, 315–316 (2004).
8. Shvets, G. Photonic approach to making a material with a negative index of refraction. *Phys. Rev.B* **67**, 035109 (2003).
9. Shin, H. & Fan, S. All-angle negative refraction for surface plasmon waves using a metal-dielectric-metal structure. *Phys. Rev. Lett.* **96**, 073907 (2006).
10. Alu, A. & Engheta, N. Optical nanotransmission lines: synthesis of planar left-handed metamaterials in the infrared and visible regimes. *J. Opt. Soc. Am. B* **23**, 571-583 (2006).

11. Lezec, H. J., Dionne, J. A. & Atwater, H. A. Negative refraction at visible frequencies. *Science* **316**, 430-432 (2007).

12. Yeh, P. *Optical Waves in Layered Media* 118-143 (Wiley, 1988).

13. Foteinopoulou, S. & Soukoulis, C. M. Negative refraction and left-handed behavior in two-dimensional photonic crystals. *Phys. Rev. B.* **67**, 235107 (2003).

14. Menzel, C. *et al.* Retrieving effective parameters for metamaterials at oblique incidence. *Phys. Rev. B* **77**, 195328 (2008).

15. Xiao, S., *et al.* Yellow light negative index metamaterials. *Opt. Lett.* **34**, 3478-3480 (2009).

16. Houck, A. A., Brock, J. B. & Chuang, I. L. Experimental observations of a left-handed material that obeys Snell's law. *Phys. Rev. Lett.* 90, 137401 (2003).

17. Grbic, A., & Eleftheriades, G. V. Overcoming the diffraction limit with a planar left-handed transmission-line lens. *Phys. Rev. Lett.* **92**, 11403 (2004).

18. Iyer, A. K. & Eleftheriades, G. V., Free-space imaging beyond the diffraction limit using a Veselago-Pendry transmission-line metamaterial superlens. *IEEE Trans. Antennas. Propag.* **57**, 1720-1727 (2009).

19. Pendry, J. B. Negative refraction makes a perfect lens. *Phys. Rev. Lett.* **85**, 3966-3969 (2000).

20. Ziolkowski, R. W. & Heyman, E. Wave propagation in media having negative perimittivity and permeability. *Phys. Rev. E* **64**, 056625 (2001).

21. Garcia N., & Nieto-Vesperinas, M., Left-handed materials do not make a perfect lens. *Phys. Rev. Lett.* **88**, 207403 (2002).

22. Loschialpo, P. F., Smith, D. L., Forester, D. W., Rachford, F. J. & Schelleng, J. Electromagnetic waves focused by a negative-index planar lens. *Phys. Rev.E* **67**, 025602 (2003).

23. Rao, X. S. & Ong, C. K. Subwavelength imaging by a left-handed material superlens. *Phys. Rev.E* **68**, 067601 (2003).

24. Nieto-Vesperinas, M. Problem of image superresolution with a negative-refractive-index slab. *J. Opt. Soc. Am. A* **21**, 491-498 (2004).

25. Fang, N., Lee, H., Sun, C. & Zhang, X. Sub-diffraction-limited optical imaging with a silver superlens. *Science* **308,** 534-537 (2005).

26. Hess, O. *et al*. Active nanoplasmonic metamaterials. *Nature Mater.* **11**, 573-584 (2012).

27. Carp, O., Huisman, C. L. & Reller, A. Photoinduced reactivity of titanium dioxide. *Prog. Solid State Chem*. **32**, 33-177 (2004).

28. Chen, X. & Mao, S. S. Titanium dioxide nanomaterials: synthesis, properties, modifications, and applications. *Chem. Rev.* 38, 2891-2959 (2007).

29. Zhang, X. Y., Dhawan, A., Wellenius, P., Suresh, A. & Muth, J. F. Planar ZnO ultraviolet modulator. *Appl. Phys. Lett.* **91**, 071107 (2007).

30. Kao, C., Bhattacharyya, A., Thomidis, C., Paiella, R., Moustakas, T. D. Electroabsorption modulators based on bulk GaN films and GaN/AlGaN multiple quantum wells. *J. Appl. Phys.* **109**, 083102 (2011).

Supplementary Information is available in the online version of the paper.

Acknowledgements We thank A. Liddle, K. Srinivasan, R. McMichael, A. Nahata and S. Blair for discussions. We also thank the staff from CNST NanoFab for technical support. T.X. and M.A. acknowledge support under the Cooperative Research Agreement between the University of Maryland and the National Institute of Standards and Technology Center for Nanoscale Science and Technology, award no. 70NANB10H193 through the University of Maryland.

Author Contributions The experiments were designed and performed by T.X., A.A., M.A. and H.J.L. Simulations were performed by T.X., M.A. and K.J.C. with further analysis by A.A. and H.J.L. All authors contributed to the interpretation of results and participated in manuscript preparation.

Author Information Reprints and permissions information is available at www.nature.com/reprints. The authors declare no competing financial interests. The authors declare no competing financial interests. Readers are welcome to comment on the online version of the paper. Correspondence and requests for materials should be addressed to H.J.L. (hlezec@nist.gov).

FIGURE CAPTIONS

Figure 1 Ultraviolet bulk metamaterial. a, Schematic of negative refraction of ultraviolet light from air into a coupled plasmonic waveguide metamaterial formed by three vertically stacked MDMDM unit cells and coated with a beam-defining mask consisting of a rectangular aperture in an opaque Cr film. S_i and S_t, incident and transmitted time-averaged Poynting vectors, respectively; k_i and k_t, incident and transmitted wavevectors, respectively. **b**, Calculated three-dimensional EFCs for an ultraviolet plane wave of free-space wavelength $\lambda_0 = 363.8$ nm in the as-designed metamaterial structure and in free space (k_0, free-space wavevector). The process of negative refraction for both the Poynting vector and the wavevector at the air–metamaterial interface is illustrated for an incident angle $\theta_i = 40°$; the conservation of the tangential wavevector component is represented by the black dash–dot line.

Figure 2 Experimental and simulated results for refraction of power and phase. a, Scanning electron microscope image of the fabricated sample used in the refraction experiment, showing the beam-defining aperture, and sectioned by focused-ion-beam (FIB) milling to reveal the internal metamaterial structure. Left inset, glass slide uniformly coated with 450-nm-thick metamaterial; right inset, magnified cross-section of the metamaterial layers. **b**, Intensity profile of transmitted beam imaged with an optical microscope at the glass–metamaterial interface and integrated over aperture length, at various incident angles θ_i, for transverse magnetic (TM) and transverse electric (TE) polarizations. **c**, Power refractive index of the metamaterial, as a function of θ_i, for TMP light. The purple points show $n_{S,Meas}$, the experimentally derived value of n_S, for which the horizontal error bars correspond to the mechanical uncertainty ($\pm 1°$) in the angle of illumination and the vertical error bars represent the uncertainty in the measured lateral shift due to the pixel resolution of the recording charge-coupled-device camera. The red dotted line shows $n_{S,EFC}$, the value of n_S derived from the metamaterial's EFC. The red solid line shows $n_{S,FDTD1}$, the value of n_S derived from FDTD simulations in which an ultraviolet beam is diffracted through an aperture-bearing metamaterial akin to that in the experiments. The red dashed line shows $n_{S,FDTD2}$, the value of n_S derived from FDTD simulations in which a plane wave is incident on a bare metamaterial and the time-averaged Poynting vector is averaged over a unit cell. Inset, simulated profile of the time-averaged Poynting vector for the aperture-bearing metamaterial

illuminated at $\theta_i = 40°$. **d**, Refractive index of the bare metamaterial, as a function of θ_i, for TMP light. The blue solid line shows n_{eff}, the refractive index derived from effective parameter retrieval applied to FDTD-simulated reflection and transmission data. The blue dotted line shows n_{EFC}, the refractive index derived from the metamaterial EFC. Inset, simulated magnetic field distribution for the metamaterial slab illuminated with a plane wave incident at $\theta_i = 40°$. The dash–dot lines show phase fronts in free space and glass, the dashed lines show effective phase fronts in the metamaterial inferred from Snell's law (on the basis of n_{eff}), and the red and green arrows represent the Poynting vector and the wavevector, respectively.

Figure 3 Ultraviolet flat lensing. a, Schematic diagram of imaging with a Veselago flat lens (of index $n = -1$ and thickness d). Optical rays diverging into the bulk of the lens from a given constituent point source on the lens surface are each negatively refracted at the exit surface of the lens, with equal and opposite ray angles on either side of the boundary, as dictated by Snell's law. This refraction process then leads all rays to converge to a point image located in free space at a distance from the exit surface equal to the thickness, *d*, of the lens. **b**, FWHM of experimental lateral intensity profile of the metamaterial flat-lens image of a 180-nm-wide slit aperture, as recorded with an optical microscope, plotted against distance, z, relative to the exit surface of the slab. The black dotted line indicates the exit surface of the lens ($z = 0$). Errors, standard deviation for repeated measurements four in total). The dashed line shows a polynomial fit. Inset, profile of the time-averaged Poynting vector resulting from FDTD simulation of the experimental configuration. The simulated transmitted beam is characterized by a waist at $z_f = 360$ nm. **c**, **d**, Scanning electron microscope images of slit apertures located on the metamaterial flat lens surface, forming cross (**c**) and ring (**d**) objects. **e**, **f**, Corresponding images produced by the flat lens under illumination by circularly polarized ultraviolet light, as recorded using an optical microscope focused at z_f. Scale bars, 3 μm. **g**, Intensity modulation contrast, γ, as a function of pump intensity at wavelengths of 290 (purple) and 760 nm (red). Pump pulse length, 150 fs; repetition rate, 80 MHz. Errors, standard deviation for repeated measurements (four in total). Inset, recorded intensity profiles of slit image at z_f with pump off (top) and pump on (bottom). Pump intensity, 18 kW cm^{-2}

Figure 1

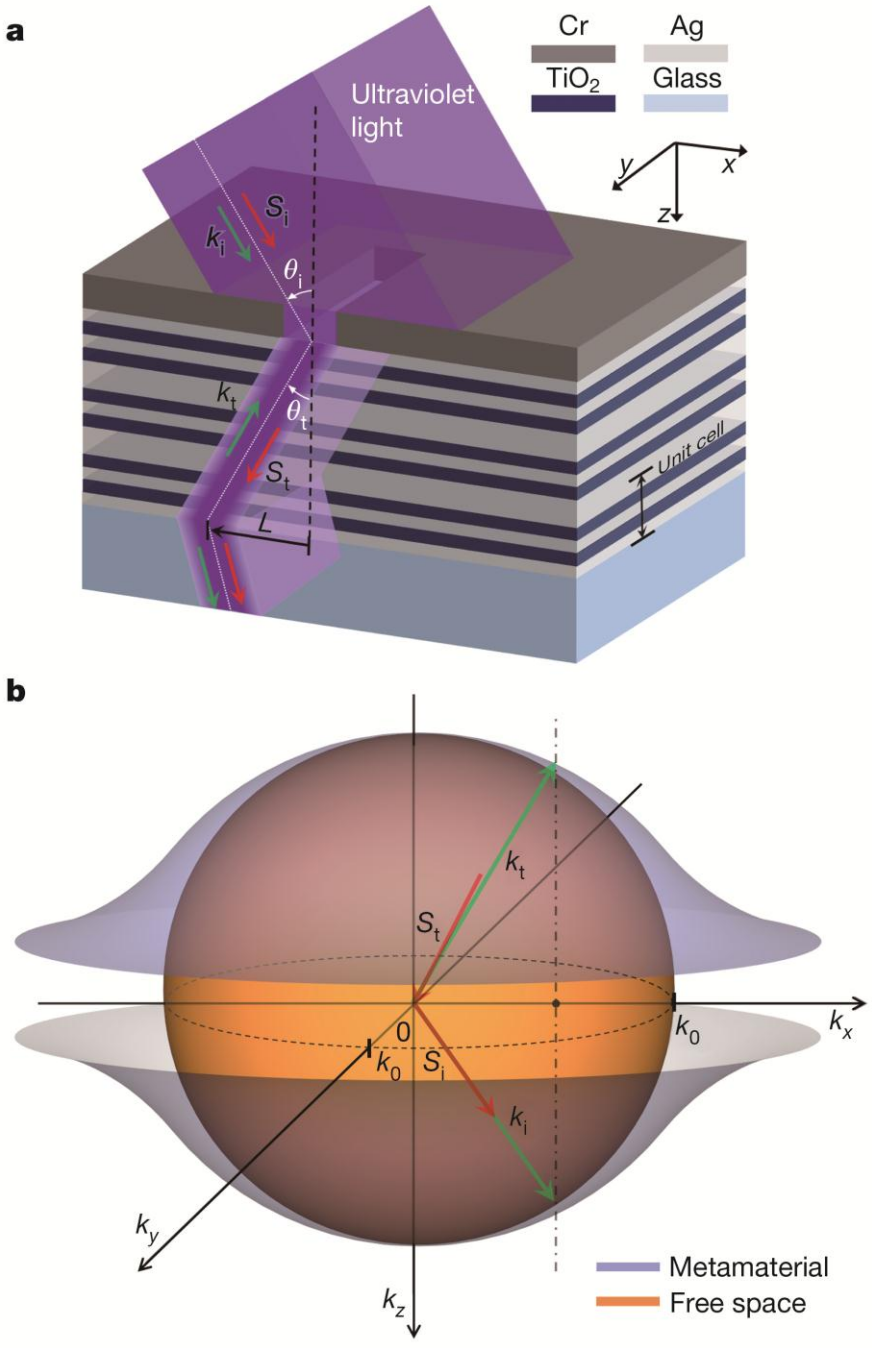
a
Cr
Ag
TiO2
Glass
Ultraviolet light
y
x
z
Si
ki
θi
kt
θt
St
L
Unit cell
b
kt
St
0
k0
Si
ki
kx
ky
kz
Metamaterial
Free space

Figure 2

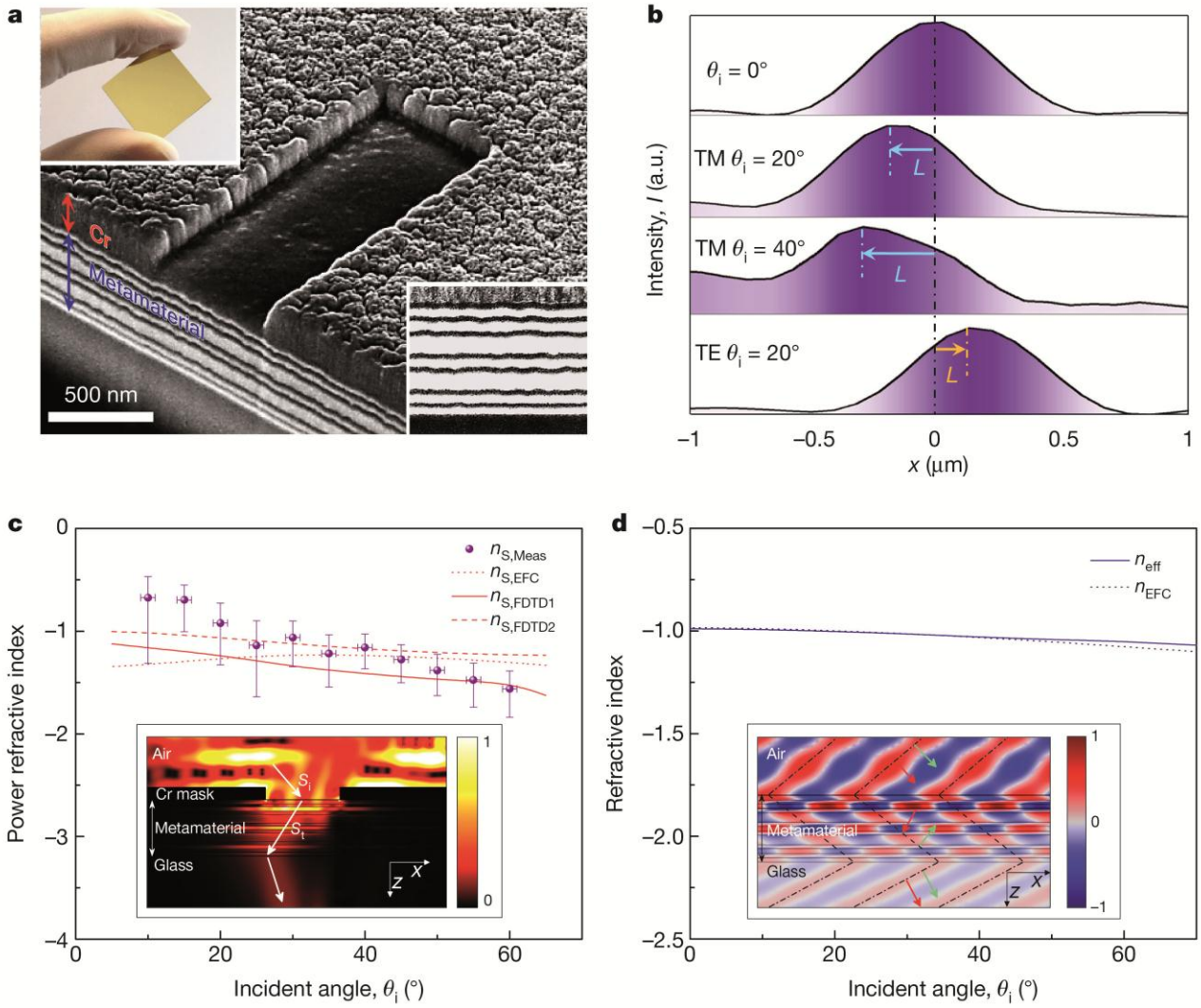
a
Cr
Metamaterial
500 nm
b
θ_i = 0°
TM θ_i = 20°
TM θ_i = 40°
TE θ_i = 20°
L
Intensity, I (a.u.)
−1
−0.5
0
0.5
1
x (μm)
c
$n_{S,Meas}$
$n_{S,EFC}$
$n_{S,FDTD1}$
$n_{S,FDTD2}$
Air
Cr mask
Metamaterial
Glass
S_i
S_t
z
x
1
0
Power refractive index
0
−1
−2
−3
−4
0
20
40
60
Incident angle, θ_i (°)
d
n_{eff}
n_{EFC}
Air
Metamaterial
Glass
z
x
1
0
−1
Refractive index
−0.5
−1.0
−1.5
−2.0
−2.5
0
20
40
60
Incident angle, θ_i (°)

Figure 3

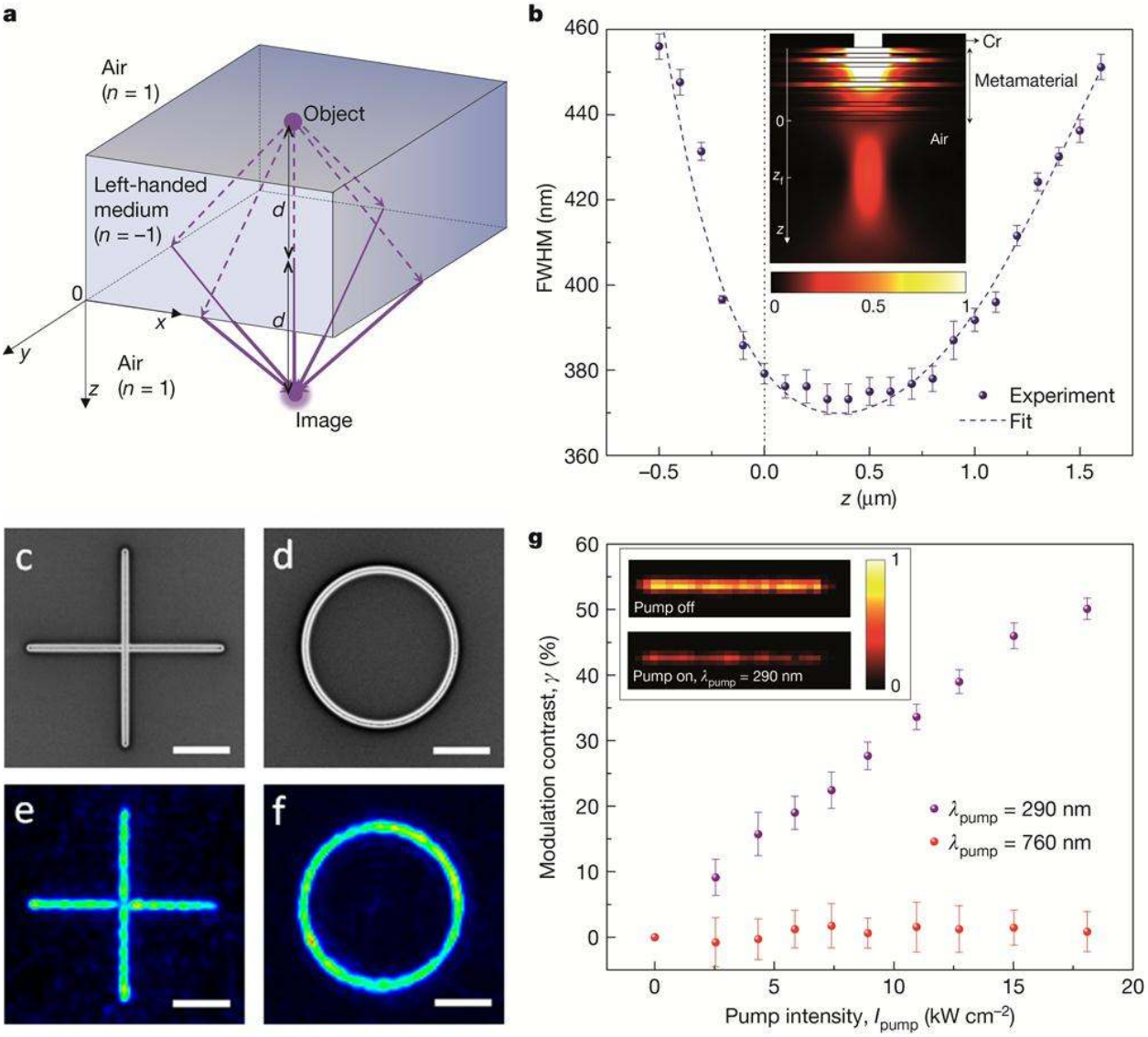
a
Air
(n = 1)
Object
Left-handed
medium
(n = −1)
d
d
0
x
y
z
Air
(n = 1)
Image
b
FWHM (nm)
460
440
420
400
380
360
−0.5
0.0
0.5
1.0
1.5
z (μm)
Cr
Metamaterial
Air
0
z_f
z
0
0.5
1
Experiment
Fit
c
d
e
f
g
Modulation contrast, γ (%)
60
50
40
30
20
10
0
0
5
10
15
20
Pump intensity, I_pump (kW cm^−2)
Pump off
Pump on, λ_pump = 290 nm
1
0
λ_pump = 290 nm
λ_pump = 760 nm

SUPPLEMENTARY INFORMATION

1. Numerical retrieval of effective parameters of metamaterial

We perform FDTD simulations of an unmasked, free-standing slab of as-designed metamaterial (thickness d = 450 nm), illuminated by a transverse-magnetic-polarized (TMP) plane-wave (λ_0 = 363.8 nm), at various angles of incidence θ_i. The refractive indices for Ag ($n = 0.0785 + 1.59\,i$) and TiO_2 ($n = 2.8 + 0.05\,i$) used in the simulations are obtained from ref. 1 and spectroscopic ellipsometry measurements, respectively. Effective parameter retrieval[2] then yields, as a function of θ_i, the complex effective electric permittivity, $\underline{\varepsilon}_{\text{eff}}$, the complex effective magnetic permeability, $\underline{\mu}_{\text{eff}}$, and the complex effective mode index, $\underline{n}_{\text{m,eff}}$ of the metamaterial (Fig. 1). The real parts of $\underline{\varepsilon}_{\text{eff}}$ (Fig. 1a) and $\underline{\mu}_{\text{eff}}$ (Fig. 1b) are simultaneously negative over the explored angular range $0^\circ \le \theta_i \le 70^\circ$, yielding a classical double-negative left-handed medium. As shown in Fig. 1c, the effective refractive index of the metamaterial, $n_{\text{eff}} = \text{Re}(\underline{n}_{\text{m,eff}})$, is negative and relatively constant over the range $0^\circ \le \theta_i \le 70^\circ$ (monotonically decreasing from −0.96 at $\theta_i = 0^\circ$ to −1.07 at $\theta_i = 70^\circ$), confirming an all-angle left-handed response characterized by a refractive index close to the targeted value of −1. The simulated figure of merit (FOM) of the metamaterial, defined as $\left|\text{Re}[\underline{n}_{\text{m,eff}}]/\text{Im}[\underline{n}_{\text{m,eff}}]\right|$, takes on a range of values (from 4 at $\theta_i = 0^\circ$ to 5.7 at $\theta_i = 70^\circ$) which are all relatively high compared to the typical FOM of conventional resonator-based metamaterials not incorporating gain media.

The imaginary parts of $\underline{\varepsilon}_{\text{eff}}$ (Fig. 1a) and $\underline{\mu}_{\text{eff}}$ (Fig. 1b) are respectively positive and negative. Like other metamaterials reported to have values of $\varepsilon'' \equiv \text{Im}(\varepsilon)$ and $\mu'' \equiv \text{Im}(\mu)$ of opposite signs[3,4], the present metamaterial seems to contradict the thermodynamic requirement of positive energy dissipation, commonly interpreted as $\varepsilon'' > 0$ and $\mu'' > 0$ (ref. 5). Recent work has suggested, however, that the condition of positive energy dissipation does not necessarily require that ε'' and μ'' be simultaneously positive[6] and that it is nonetheless possible to satisfy thermodynamic requirements while still having one of ε'' or μ'' be negative.

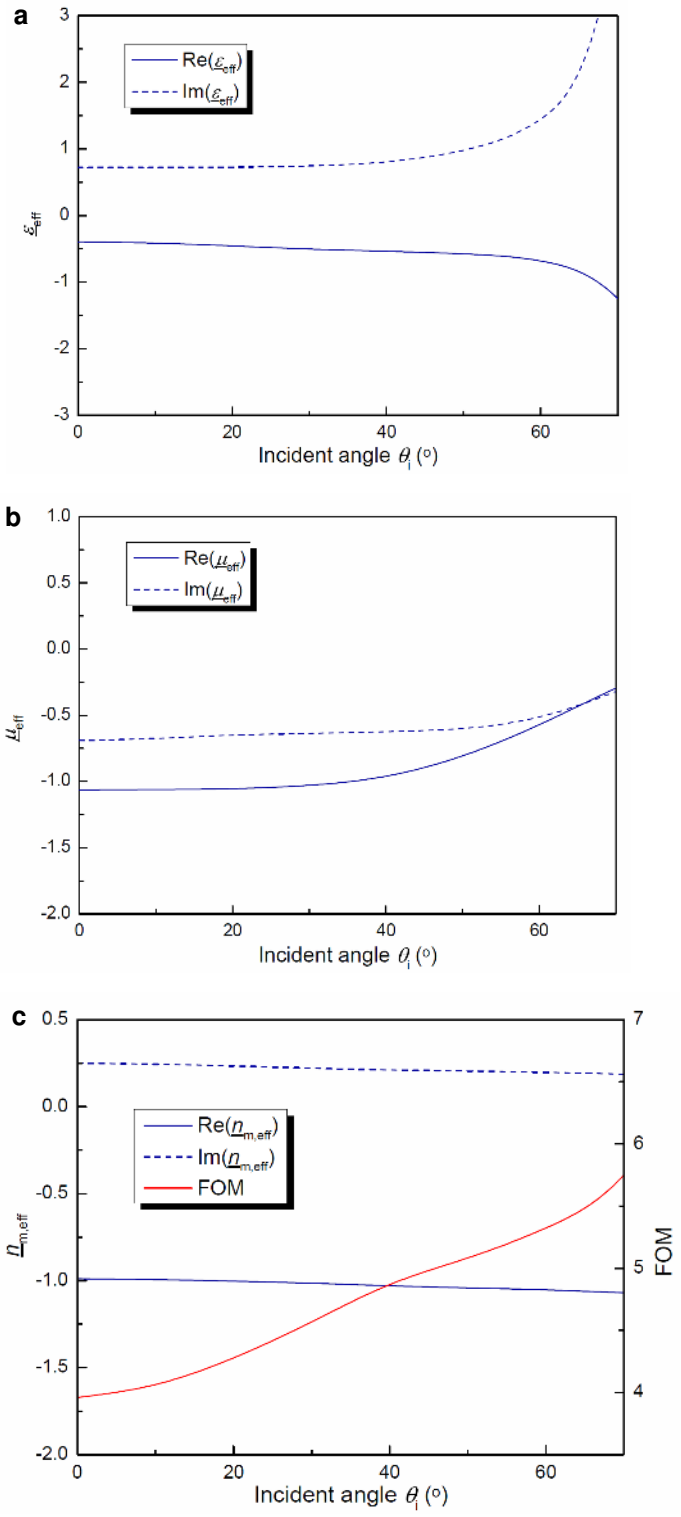

Figure 1 | Retreived effective medium parameters of metamaterial. a, Complex effective permittivity, $\underline{\varepsilon}_{\text{eff}}$. **b,** complex effective permeability, $\underline{\mu}_{\text{eff}}$. **c,** complex effective mode index, $\underline{n}_{\text{m,eff}}$ (left-axis), and corresponding figure of merit, FOM (right-axis), plotted as a function of incident angle θ_i . TMP illumination. Wavelength: λ_0 = 363.8 nm.

2. Simulated resolution limit of implemented flat-lens

The theoretical resolution limit of the experimentally-implemented flat lens is investigated via FDTD simulations of a free-standing slab of as-designed metamaterial (thickness d = 450 nm) illuminated at normal incidence by a plane-wave source (λ_0 = 363.8 nm) of subwavelength width, w_s, placed directly on the input surface of the slab. The refractive indices assumed for the constituent Ag and TiO_2 layers are identical to those quoted in the previous section. The image of the truncated plane wave projected by the flat lens is characterized for values of w_s spanning the range 30 to 300 nm. The simulated total energy density reveals an image beam waist located at a distance z_f = 360 nm from the lens exit surface. The image width, $w_{f,FDTD}$, defined as the FWHM of the energy-density waist at z_f, is plotted in Fig. 2 as a function of w_s. As the source-width w_s decreases towards zero, the image width $w_{f,FDTD}$ decreases towards a limit of $\approx$190 nm. This value is larger than, but relatively close to the minimum image width of 161 nm (FWHM) theoretically predicted to result when a line source of infinitesimal width is imaged at $\lambda_0 = 363.8$ nm by a free-space diffraction-limited system having a maximal value of numerical aperture (N.A. = 1).

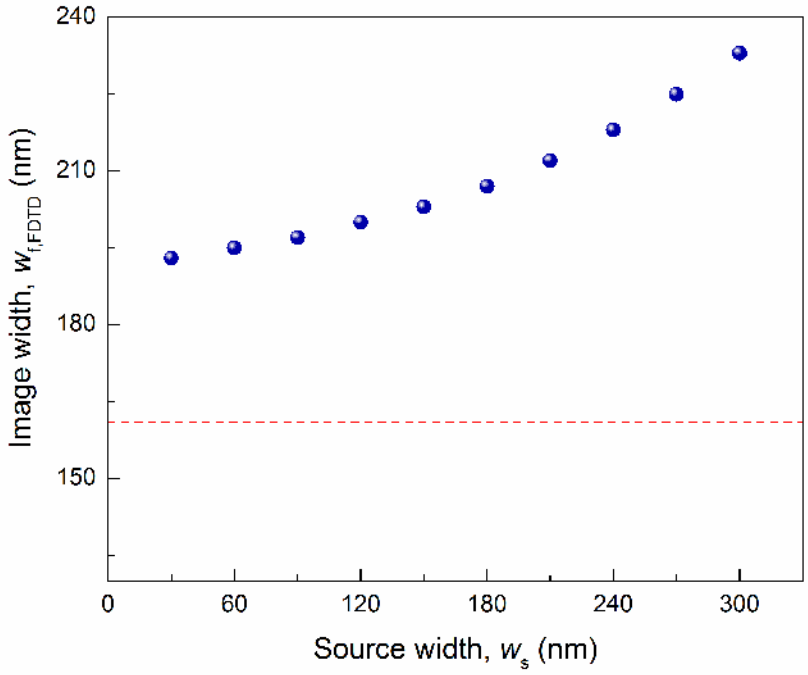

Figure 2 | Simulated resolution of the flat lens. The blue dots show the FDTD-simulated image width, $w_{f,FDTD}$, as a function of source width, w_s. The red dashed line indicates the predicted image width for a line source imaged by a diffraction-limited system with N.A. = 1. Lens thickness: d = 450 nm. Operating wavelength: λ_0 = 363.8 nm.

3. Active flat lensing: TiO_2 optical properties and experimental setup

To infer the bandgap of the TiO_2 semiconducting material incorporated in the experimental flat lens, a UV-Visible spectrometer was used to measure the optical absorbance spectrum of a 50nm-thick TiO_2 reference film sputter-deposited onto a fused-quartz slide (Fig. 3a). The onset of a distinct absorption-edge is observed at a wavelength of $\approx$ 350 nm (as a function of decreasing wavelength), implying an experimental TiO_2 bandgap of value $E_{BG} \approx 3.54$ eV.

Fig. 3b shows the schematic diagram of the experimental setup used to demonstrate active flat lensing. To generate free carriers to suppress the optical transmission of the metamaterial slab at its designed working wavelength of 363.8 nm, an above-bandgap pump beam of wavelength $\lambda_{pump} = 290$ nm is chosen. In a control experiment intended to verify the lack of transmission suppression in the absence of optically-generated free carriers, a sub-bandgap pump beam of wavelength $\lambda_{pump} = 760$ nm is used instead.

Supplementary References

1. Johnson, P. B. & Christy, R. W., Optical constants of the noble metals. *Phys. Rev. B* **6**, 4370-4379 (1972).

2. Menzel, C. *et al.* Retrieving effective parameters for metamaterials at oblique incidence. *Phys. Rev. B* **77**, 195328 (2008).

3. Markos, P. & Soukoulis, C. M., Transmission properties and effective electromagnetic parameters of double negative metamaterials, *Opt. Express* 11, 649-661 (2003).

4. Burgos, S. P., Waele, R., Polman, A. & Atwater, H. A. A single-layer wide-angle negative-index metamaterial at visible frequencies. *Nat. Mater.* **9**, 407-412 (2010).

5. Landau, L. D., Pitaevskiĭ, L. P. & Lifshitz, E. M., Electrodynamics of Continuous Media, 2nd Edition, 272-274, *Pergamon Press*, New York (1984).

6. Koschny, T., Markos, P., Smith, D. R. & Soukoulis, C. M., Resonant and antiresonant frequency dependence of the effective parameters of metamaterials. *Phys. Rev. E* **68**, 065602(R) (2003).

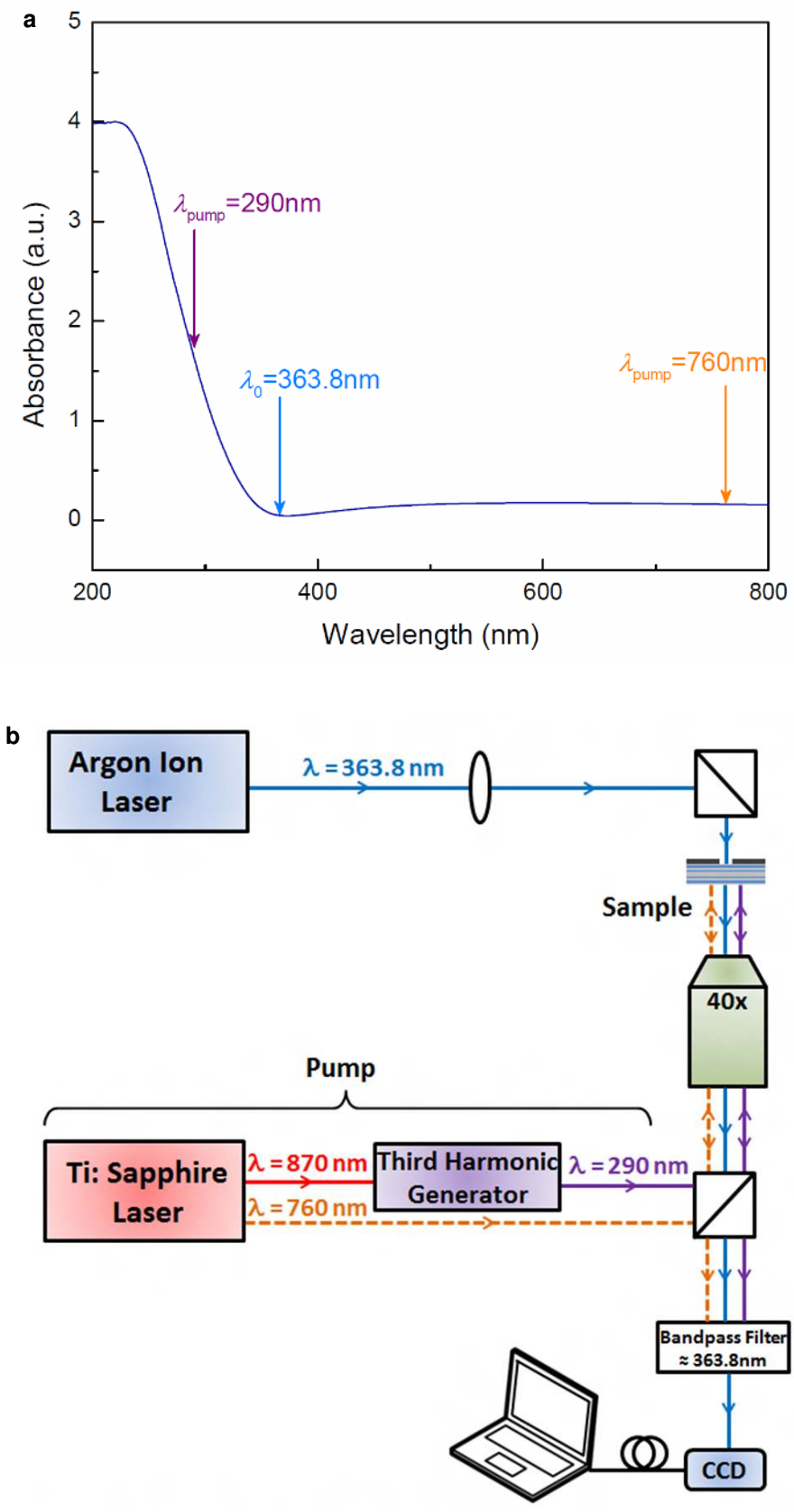

Figure 3 | Active Flat Lensing Experiment. a, Measured absorbance of 50nm-thick TiO_2 film, using UV-Visible spectrometer. **b,** Schematic of experimental setup used to demonstrate active flat lensing.